DALTON
FULL PAPER

Copper complexes of 2,6-bis(iminomethyl)pyridine derivatives and of 1,3-bis(pyridin-2-yl)pyrazole. Effects of ligand bulk and conformational strain on the ground state of a six-co-ordinate copper(II) ion

Joanne M. Holland,[a] Xiaoming Liu,[a] Jing P. Zhao,[b] Frank E. Mabbs,[b] Colin A. Kilner,[a] Mark Thornton-Pett[a] and Malcolm A. Halcrow*[a]

[a] *School of Chemistry, University of Leeds, Woodhouse Lane, Leeds, UK LS2 9JT. E-mail: M.A.Halcrow@chem.leeds.ac.uk*
[b] *CW EPR Service Centre, Department of Chemistry, University of Manchester, Oxford Road, Manchester, UK M13 9PL*

Received 26th June 2000, Accepted 2nd August 2000
First published as an Advance Article on the web 18th September 2000

Complexation of hydrated $Cu(BF_4)_2$ by 2 molar equivalents of L^2R (L^2Me = 2,6-bis{methyliminomethyl}-pyridine, L^2Cy = 2,6-bis{cyclohexyliminomethyl}pyridine, L^2Bu^t = 2,6-bis{*tert*-butyliminomethyl}pyridine) afforded $[Cu(L^2R)_2][BF_4]_2$ (R = Me, **1**; Cy, **2**; or Bu^t, **3**) in moderate yields. EPR spectroscopy in solution and the solid state demonstrates that **1** and **2** adopt the expected $\{d_{x^2-z^2}\}^1$ electronic ground state, and that the pseudo-Jahn–Teller elongation axis is fluxional in solid **1** and static in solid **2**. In contrast, **3** exhibits a $\{d_{z^2}\}^1$ ground state by EPR. The crystal structures of **2**·$MeNO_2$ and **3**·$\frac{1}{2}Me_2CO$ contain rhombic six-co-ordinate copper(II) ions, which differ principally in the length of the Cu–N bonds close to the molecular *y* axis. Treatment of $[Cu(NCMe)_4]$-BF_4 with varying ratios of L^2R yields $[Cu(L^2R)_2]BF_4$ (R = Me, **4**; Mes, **5**; or Cy, **6**: L^2Mes = 2,6-bis{2,4,6-trimethylphenyliminomethyl}pyridine) or $[\{Cu(L^2Bu^t)\}_2][BF_4]_2$ **7**. The single crystal structure of **5**·MeCN shows a flattened tetrahedral copper(I) centre with two bidentate L^2Mes ligands. Reaction of hydrated $Cu(ClO_4)_2$ with 2 molar equivalents of L^3 (1,3-bis{pyridin-2-yl}pyrazole) yields $[Cu(L^3)_2][ClO_4]_2$ **8**, whose crystal structure demonstrates a six-co-ordinate copper(II) ion with long Cu–N{pyridine} bonds. Powder EPR spectroscopy demonstrates a $\{d_{z^2}\}^1$ ground state for **8** in the solid.

Introduction

The Jahn–Teller effect[1] in $[CuL_2]^{2+}$ (L = meridional tridentate ligand) complexes manifests itself as an elongation along the molecular *x* axis (Scheme 1), affording a $\{d_{y^2-z^2}\}^1$ electronic ground state. In the solid state this elongation is often dynamically disordered over the molecular *x* and *y* axes, which leads to unusual, temperature-dependent EPR behaviour.[2–6] We have discovered that a unique change in ground state can be enforced at the complexes $[Cu(L^1R)_2]^{2+}$ by introduction of bulky 'R' substituents, which sterically inhibit this Jahn–Teller fluxionality through steric interactions between the 'R' groups on one ligand and the backbone of the other perpendicular one (Scheme 1).[5,7] Hence, $[Cu(L^1H)_2]^{2+}$ shows the usual $\{d_{y^2-z^2}\}^1$ ground state by EPR spectroscopy, while $[Cu(L^1Mes)_2]^{2+}$ adopts a $\{d_{z^2}\}^1$ ground state, which should correspond structurally to a compression along the molecular *z* axis (Scheme 1, A).[7] A meaningful structural comparison of the two compounds was impossible, however, because the solid state fluxionality shown by $[Cu(L^1H)_2]^{2+}$ [5,6] prevents its true Cu–N distances from being determined.[8]

There is only one previous example of a 6-co-ordinate, tetragonally compressed copper(II) centre with a homoleptic donor set, in the co-ordination polymer $KAlCuF_6$.[9] We therefore wished to examine the generality of our result, by preparing copper(II) complexes of other meridional tridentate ligands whose distal steric bulk could readily be modified. We describe here the syntheses, structures and spectroscopy of a series of complexes $[Cu(L^2R)_2]^{2+}$ (R = Me, Cy or Bu^t). Included in this work are the crystal structures of $[Cu(L^2Cy)_2][BF_4]_2$ and $[Cu(L^2Bu^t)_2][BF_4]_2$, which for the first time allow a genuine structural comparison between copper(II) complexes with identical ligand donors that exhibit different electronic ground states. The copper(I) complex chemistry of these and other L^2R ligands is also presented. Finally, we report the properties of $[Cu(L^3)_2]^{2+}$, which was synthesized with a view to obtaining a 6-co-ordinate $\{d_{z^2}\}^1$ copper(II) complex without the use of bulky ligand substituents. The molecular axis convention shown in Scheme 1 is used throughout the following discussion; in those crystal structures that show a rhombic stereochemistry, the long, medium and short Cu–N bonds are assumed to lie close to the molecular *x*, *y* and *z* axes, respectively.

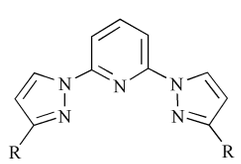

L^1R
(R = H, Pr^i, Ph, Mes)

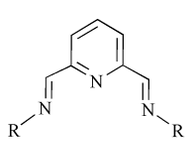

L^2R
(R = Me, Ph, Mes, Cy, Bu^t)

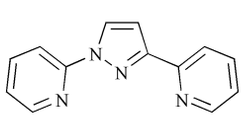

L^3

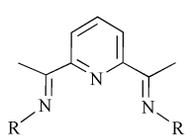

L^4R

Results and discussion

Copper(II) complexes of L^2R

Surprisingly few $[M(L^2R)_2]^{n+}$ (M^{n+} = transition ion) complexes have been reported previously,[10–13] and no $[Cu(L^2R)_2]^{2+}$

 DOI: 10.1039/b005105p

Table 1 Selected Q-band EPR data for the copper(II) complexes in this study. Solution spectra were run in 10:1 MeCN–toluene. Spectra with two identical g values have axial symmetry. All hyperfine couplings are to ^{63,65}Cu and are in G. Estimated errors in these parameters are $g \pm 0.002$, $A \pm 2$ G

	Phase	T/K	g_1	g_2	g_3	A_1	A_2	A_3
1 $[Cu(L^2Me)_2][BF_4]_2$[a]	Powder	292	2.179	2.153	2.068	—	—	—
		110	2.176	2.133	2.068	—	—	—
		5[b]	2.182	2.090	2.060	—	—	—
			2.230	2.230	2.090	—	—	—
2 $[Cu(L^2Cy)_2][BF_4]_2$	Powder	292	2.252	2.083	2.043	135	—	—
		110	2.252	2.081	2.042	144	—	—
		10	2.256	2.073	2.040	154	—	—
	MeCN	110	2.252	2.081	2.042	144	—	—
3 $[Cu(L^2Bu^t)_2][BF_4]_2$	Powder	292	2.231	2.202	2.005	—	—	155
		110	2.231	2.202	2.000	—	—	155
		10	2.219	2.219	1.998	—	—	161
	MeCn	110	2.220	2.215	2.001	—	—	165
8 $[Cu(L^3)_2][ClO_4]_2$[a]	Powder	292	2.220	2.196	2.011	—	—	141
		117	2.220	2.200	2.004	—	—	155
		10	2.221	2.221	2.001	—	—	170

[a] The spectrum of this compound in MeCN at 110 K is poorly resolved, and could not be simulated accurately. See text for details. [b] Two signals present in the spectrum, in approximately equal proportions. See text for details.

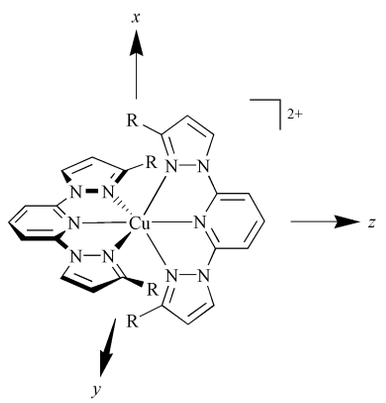

A

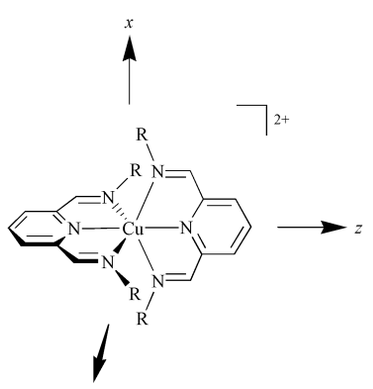

B

Scheme 1 Molecular axes for $[Cu(L^1R)_2]^{2+}$ (A) and $[Cu(L^2R)_2]^{2+}$ (B).

complex has previously been characterised by EPR spectroscopy. In addition, we are only aware of two literature reports of $[Cu(L^4R)_2]^{2+}$ complexes, whose EPR spectra were also not measured.[14] However, we noted that the d^9 species $[Ni(L^4Bz)_2]^+$ (Bz = benzyl) shows a $\{d_{y^2-z^2}\}^1$ ground state by EPR spectroscopy.[15] Hence, it seemed that R substituents more bulky than benzyl would be required in $[Cu(L^2R)_2]^{2+}$ to cause inter-ligand repulsions of the type shown by $[Cu(L^1R)_2]^{2+}$ (Scheme 1). As a control, the complex $[Cu(L^2Me)_2]^{2+}$ was also prepared.

The ligands L^2Ph[10,16] and L^2Bu^t [17] have been reported previously. Other L^2R ligands (R = Me, Mes {mesityl} or Cy {cyclohexyl}) were prepared by reaction of pyridine-2,6-dicarbaldehyde with an excess of the appropriate amine at room temperature or in refluxing methanol. Complexation of $Cu(BF_4)_2 \cdot 6H_2O$ by 2 equivalents of L^2Me, L^2Cy or L^2Bu^t in MeCN yielded green solutions, from which green microcrystalline products could be obtained in moderate yields by addition of diethyl ether. These microcrystals analysed as the desired complexes $[Cu(L^2R)_2][BF_4]_2$ (R = Me, **1**; Cy, **2**; or Bu^t, **3**), while FAB mass spectrometry showed a highest molecular ion corresponding to the fragment $[^{63}Cu(L^2R)_2]^+$ (R = Me, m/z = 385; Cy, 657; Bu^t, 553). While **2** and **3** could be crystallised from $MeNO_2$, MeCN or acetone by vapour diffusion with Et_2O, **1** could only be obtained as a solid from MeCN–Et_2O. Analogous complexations employing L^2Ph or L^2Mes afforded deep brown solutions, from which no clean solid products could be isolated (see below).

In addition to $\pi \longrightarrow \pi^*$ absorptions in the UV region, two d–d peaks are apparent in the UV/vis spectra of complexes **1** and **2** in MeCN at 298 K,[18] at λ_{max} = 709 (ε_{max} = 48 {**1**} or 61 {**2**} M^{-1} cm^{-1}) and *ca.* 480 nm (sh). These are very close to those shown by $[Cu(L^4R)_2]^{2+}$ complexes in solution.[14] The higher wavelength band lacks a high-wavelength shoulder, which is typical for six-co-ordinate copper(II) centres.[18] That **1** and **2** exhibit identical d–d maxima suggests the cyclohexyl substituents in the latter compound are not sufficiently bulky to cause inter-ligand steric repulsions of the type shown by $[Cu(L^1R)_2]^{2+}$ (R = Pr^i, Ph or Mes). However, for **3** a single higher wavelength d–d absorption was observed, at λ_{max} = 746 nm (ε_{max} = 63 M^{-1} cm^{-1}), showing that the ligand *tert*-butyl substituents do perturb the copper ion. For all three complexes these absorptions have essentially identical wavelengths and intensities in MeCN and in $MeNO_2$, which demonstrates that minimal ligand dissociation occurs in these solvents.

All EPR spectra in this study were run at Q-band. In 10:1 MeCN–toluene solution at 120 K, complex **1** affords a broad spectrum that can be simulated with $g_1 = 2.22$, $g_2 = 2.10$, $g_3 = 2.07$, with peak-to-peak linewidths of 400 G on g_1 and g_2. This $g_1 > g_2 \approx g_3 > g_e$ pattern is characteristic for a pseudo-Jahn–Teller elongated copper(II) complex with a $\{d_{y^2-z^2}\}^1$ ground state.[19] The powder EPR spectrum of **1** is more complex, however. At 290 K an 'inverse' $g_1 \approx g_2 > g_3 > g_e$ spectrum is observed (Table 1). As the temperature is lowered this spectrum becomes more rhombic, which mostly reflects a lowering of g_2. No hyperfine coupling is apparent at any temperature. This behaviour is similar to that exhibited by $[Cu(terpy)_2][PF_6]_2$[2] and $[Cu(L^1H)_2][BF_4]_2$[5] in the powder, and is diagnostic of a $\{d_{y^2-z^2}\}^1$ copper(II) complex, whose pseudo-Jahn–Teller elongation axis is fluxional in the solid state.[1,7] Below 20 K the spectrum cannot be simulated by a single copper(II) spin; a

Table 2 Selected bond lengths (Å) and angles (°) at copper in the single crystal structure of $[Cu(L^2Cy)_2][BF_4]_2 \cdot MeNO_2$ **2**·$MeNO_2$

Cu(1)–N(1)	1.936(2)	Cu(1)–N(4)	2.004(2)
Cu(1)–N(2)	2.085(2)	Cu(1)–N(5)	2.412(2)
Cu(1)–N(3)	2.091(2)	Cu(1)–N(6)	2.443(2)
N(1)–Cu(1)–N(2)	79.02(9)	N(2)–Cu(1)–N(6)	96.73(8)
N(1)–Cu(1)–N(3)	78.70(9)	N(3)–Cu(1)–N(4)	101.79(8)
N(1)–Cu(1)–N(4)	178.94(9)	N(3)–Cu(1)–N(5)	98.09(8)
N(1)–Cu(1)–N(5)	105.61(8)	N(3)–Cu(1)–N(6)	87.27(8)
N(1)–Cu(1)–N(6)	104.67(9)	N(4)–Cu(1)–N(5)	75.28(8)
N(2)–Cu(1)–N(3)	157.65(9)	N(4)–Cu(1)–N(6)	74.45(8)
N(2)–Cu(1)–N(4)	100.46(9)	N(5)–Cu(1)–N(6)	149.72(8)
N(2)–Cu(1)–N(5)	89.51(8)		

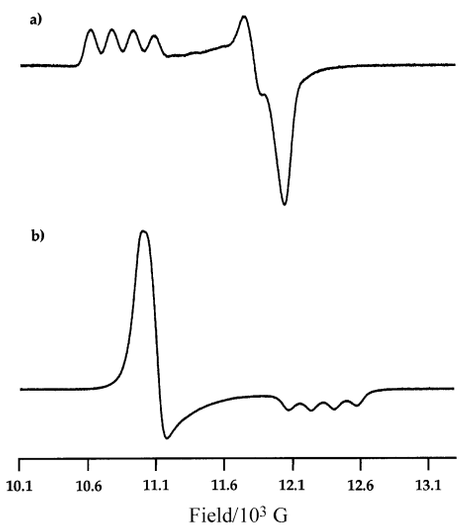

Fig. 1 Q Band powder EPR spectra at 10 K of: (a) complex **2**; (b) **3**.

better simulation of the spectrum profile at 5 K is obtained assuming two species in approximately equal proportions. One of these signals affords g values that resemble those of **1** in frozen solution, while the other signal has an apparently axial 'inverse' g pattern (Table 1). Hence, we suggest that at $T \leq 20$ K we observe a combination of exchange-averaged crystal and resolved molecular spectra from this sample.

The EPR spectra of complexes **2** and **3**, while differing between the two, are virtually identical in the powder and in frozen MeCN, and show only small variations with temperature in the powder (Table 1). This shows that these complexes have static structures in the solid, and that their molecular and electronic structures in the solid state and in solution are the same. For **2**, the EPR spectra in both phases are rhombic and exhibit a $g_1 > g_2 \approx g_3 > g_e$ pattern (Fig. 1a). This shows that, like **1**, **2** possesses a tetragonally elongated $\{d_{y^2-z^2}\}^1$ copper(II) centre. However, for **3** the EPR spectra are almost axial with $g_1 \approx g_2 > g_3 \approx g_e$, which is consistent with a $\{d_{z^2}\}^1$ ground state (Fig. 1b).[19] The alternative description of solid **3**, as a fluxional $\{d_{y^2-z^2}\}^1$ species akin to **1**, is ruled out because $g_3 \approx g_e$, and because an almost identical spectrum is obtained in frozen solution. Therefore, in contrast to **1** and **2**, **3** must be formulated either as a tetragonally compressed 6-co-ordinate complex, or as a trigonal bipyramidal copper(II) centre with one non-co-ordinated imine donor. The former scenario was confirmed by the single crystal structure analysis described below.

Structural analyses were accomplished on single crystals of composition **2**·$MeNO_2$ and **3**·$\frac{1}{2}Me_2CO$. Both complexes exhibit rhombically distorted octahedral stereochemistries (Figs. 2 and 3, Tables 2 and 3). The $[Cu(L^2Cy)_2]^{2+}$ dication in **2** shows a clear axis of elongation along the N(5)–Cu(1)–N(6) vector, while the Cu–N bonds along the molecular y axis [N(2)–Cu(1)–N(3)] are only slightly longer than the z axis [N(1)–Cu(1)–N(4)] (Fig. 2, Table 2). This supports the conclusion that

Table 3 Selected bond lengths (Å) and angles (°) at copper in the single crystal structure of $[Cu(L^2Bu^t)_2][BF_4]_2 \cdot \frac{1}{2}Me_2CO$ **3**·$\frac{1}{2}Me_2CO$

Molecule 1		Molecule 2	
Cu(1)–N(1)	1.932(2)	Cu(2)–N(7)	1.927(2)
Cu(1)–N(2)	2.295(2)	Cu(2)–N(8)	2.278(2)
Cu(1)–N(3)	2.304(2)	Cu(2)–N(9)	2.313(2)
Cu(1)–N(4)	1.958(2)	Cu(2)–N(10)	1.934(2)
Cu(1)–N(5)	2.312(2)	Cu(2)–N(11)	2.352(2)
Cu(1)–N(6)	2.450(2)	Cu(2)–N(12)	2.349(2)
N(1)–Cu(1)–N(2)	77.68(6)	N(7)–Cu(2)–N(8)	78.33(7)
N(1)–Cu(1)–N(3)	77.48(6)	N(7)–Cu(2)–N(9)	77.29(7)
N(1)–Cu(1)–N(4)	176.09(7)	N(7)–Cu(2)–N(10)	178.84(7)
N(1)–Cu(1)–N(5)	106.18(6)	N(7)–Cu(2)–N(11)	102.67(6)
N(1)–Cu(1)–N(6)	100.81(6)	N(7)–Cu(2)–N(12)	102.92(6)
N(2)–Cu(1)–N(3)	155.16(6)	N(8)–Cu(2)–N(9)	155.62(6)
N(2)–Cu(1)–N(4)	103.26(6)	N(8)–Cu(2)–N(10)	102.82(7)
N(2)–Cu(1)–N(5)	92.97(6)	N(8)–Cu(2)–N(11)	90.49(6)
N(2)–Cu(1)–N(6)	93.84(6)	N(8)–Cu(2)–N(12)	92.75(6)
N(3)–Cu(1)–N(4)	101.56(6)	N(9)–Cu(2)–N(10)	101.56(6)
N(3)–Cu(1)–N(5)	93.32(6)	N(9)–Cu(2)–N(11)	94.42(6)
N(3)–Cu(1)–N(6)	91.38(6)	N(9)–Cu(2)–N(12)	93.06(6)
N(4)–Cu(1)–N(5)	77.62(7)	N(10)–Cu(2)–N(11)	77.23(6)
N(4)–Cu(1)–N(6)	75.38(6)	N(10)–Cu(2)–N(12)	77.22(6)
N(5)–Cu(1)–N(6)	152.99(6)	N(11)–Cu(2)–N(12)	154.33(6)

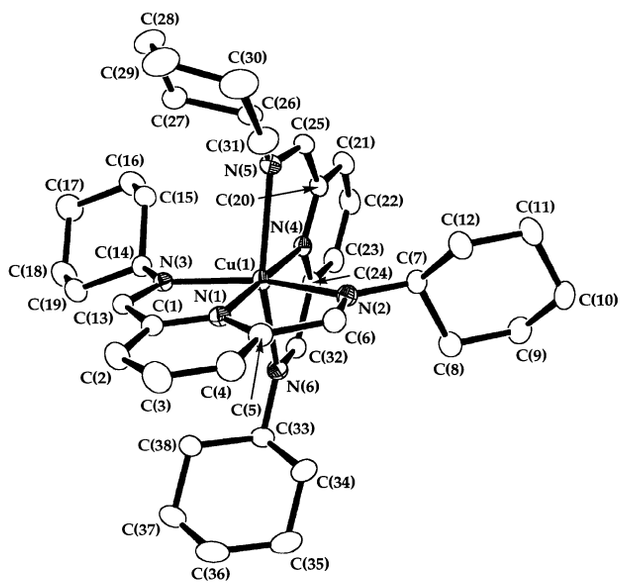

Fig. 2 View of the $[Cu(L^2Cy)_2]^{2+}$ dication in the crystal of **2**·$MeNO_2$, showing the atom numbering scheme employed. For clarity, all H atoms have been omitted. Thermal ellipsoids are drawn at the 35% probability level.

the Jahn–Teller distortion in solid **2** is static rather than dynamic, in keeping with the EPR data. The Cu(1)–N(4) distance [2.004(2) Å] is longer than Cu(1)–N(1) [1.936(2) Å], which presumably reflects increased conformational strain within the former ligand backbone caused by the lengthened Cu–N(5) and Cu–N(6) bonds. The ligand imine functions exhibit indistinguishable C=N bond lengths between 1.268(4) and 1.280(3) Å, despite the wide variation in Cu–N{imine} distances of 2.085(2)–2.443(2) Å. This suggests that there is only weak Cu→π*{N=C} back donation in this complex.

Comparison of the two structures is hampered by the fact that complex **3**·$\frac{1}{2}Me_2CO$ contains two crystallographically independent cations, whose Cu–N bond lengths show some differences, particularly along the molecular x axis (Fig. 3, Table 3). This suggests that the co-ordination sphere in **3** is rather plastic in solution. However, the near invariance of the solid state EPR spectrum of **3** with temperature,[2–5] and the almost identical and near-spherical anisotropic thermal parameters exhibited by all twelve N atoms in the structure (Fig. 3),[1] both

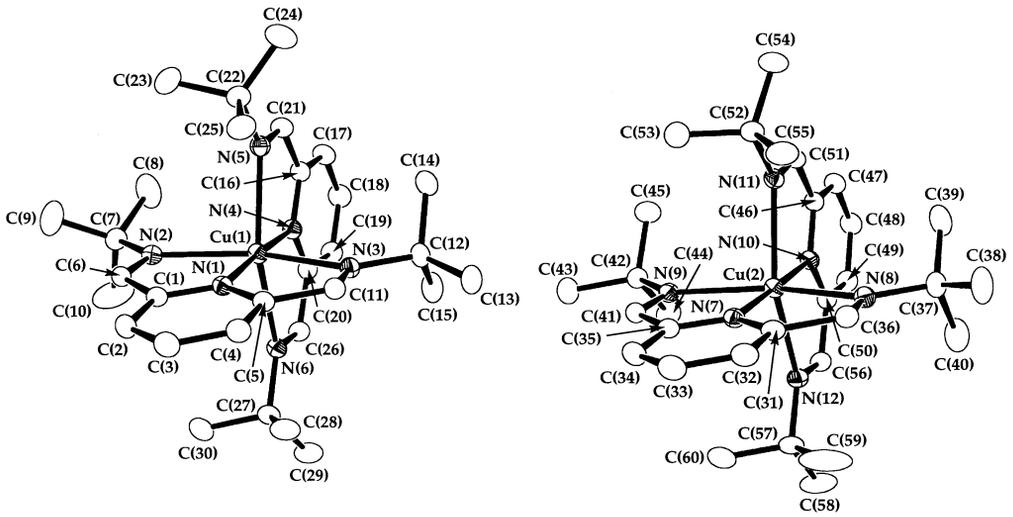

Fig. 3 Views of the crystallographically independent $[Cu(L^2Bu^t)_2]^{2+}$ dications in the asymmetric unit of $3\cdot\frac{1}{2}Me_2CO$. Details as for Fig. 2.

imply that **3** is not fluxional in the solid state. Therefore, comparison of the metric parameters at copper in **2** and **3** is justified. It is clear that, in **3**, the Cu–N bond lengths along the molecular *x* and *y* axes have converged compared to **2**; this has mostly been achieved through an elongation of the *y*-axis Cu–N bonds by 0.193(3)–0.222(3) Å. In contrast, the *z*-axis Cu–N bonds in **3** are only 0.004(3)–0.070(3) Å shorter than in **2**. Hence, the structural distortion in **3** might better be described as an elongation of the co-ordination sphere within the *xy* plane, rather than as a *z*-axis compression.

Copper(I) complexes of L^2R

As described above, our attempted syntheses of $[Cu(L^2R)_2][BF_4]_2$ (R = Ph or Mes) were unsuccessful, yielding brown solutions from which no pure solid products could be obtained. We suggested that this may reflect spontaneous reduction of the hydrated $Cu(BF_4)_2$ starting material to Cu^I in the reaction mixture, in the presence of the L^2R ligands, which should have enhanced π-acceptor capability with aryl 'R' substituents. In order to test this theory, the copper(I) complex chemistry of the L^2R ligands was examined.

Complexation of $[Cu(NCMe)_4]BF_4$ by L^2R (R = Me, Mes or Cy) in MeCN or $MeNO_2$ in all cases yielded deep brown solutions, from which brown microcrystalline solids could be isolated upon addition of Et_2O. On the basis of microanalytical data, these complexes were formulated as $[Cu(L^2R)_2]BF_4$ (R = Me, **4**; Mes, **5**; or Cy, **6**). This was supported by IR spectroscopy, which demonstrated the presence of L^2R and BF_4^- only, and by FAB mass spectrometry which showed highest molecular ions corresponding to $[^{63}Cu(L^2R)_2]^+$ (**4**, *m*/*z* = 385; **5**, 801; **6**, 657). An analogous reaction employing L^2Ph also yielded a brown solid, that gave a highest mass peak at *m*/*z* 633, corresponding to $[^{63}Cu(L^2Ph)_2]^+$. However, despite the clean mass spectrum, the microanalysis was consistently low in C, H and N, suggesting contamination by a copper(II) species.

In contrast to the above results, treatment of $[Cu(NCMe)_4]BF_4$ with L^2Bu^t under the above conditions affords a red microcrystalline powder (**7**) which analysed consistently for '$[Cu(L^2Bu^t)]BF_4\cdot H_2O$'. Importantly, the FAB mass spectrum of **7** displayed a highest mass peak at *m*/*z* = 616, corresponding to $[\{^{63}Cu(L^2Bu^t)\}_2]^+$. Therefore, **7** was formulated as a dimeric complex containing the $[\{Cu(L^2Bu^t)\}_2]^{2+}$ dication, which probably adopts a helical structure similar to those of $[\{Cu(L^1R)\}_2]^{2+}$,[20] $[\{Cu(terpy)\}_2]^{2+}$[21] or related compounds.[22,23] Presumably, the steric bulk of the Bu^t substituents prevents the formation of $[Cu(L^2Bu^t)_2]^+$. Preparations of **4**–**7** employing varying Cu : L^2R ratios of between 1 and 2 : 1 affected the yields, but not the identities, of the products obtained.

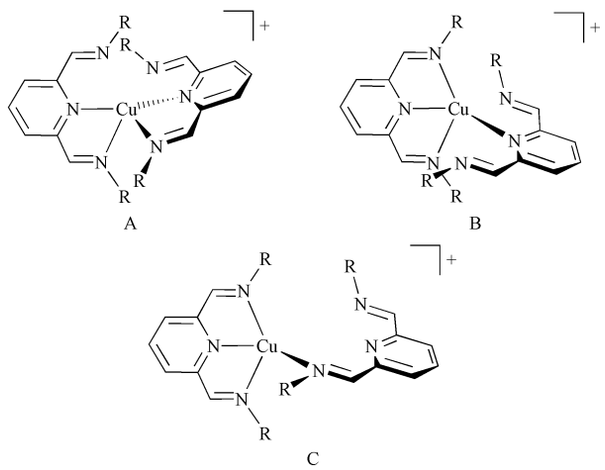

Scheme 2 Possible molecular structures for $[Cu(L^2R)_2]^+$ (R = Me, Mes or Cy), assuming 4-co-ordination at copper.

Assuming 4-co-ordination at copper, there are three possible structural isomers for $[Cu(L^2R)_2]^+$ (Scheme 2), which in principle could be distinguished by NMR spectroscopy. At room temperature, **4**–**6** (and **7**) each afford sharp ^1H NMR spectra in $CDCl_3$, showing only one C_2 or *m*-symmetric L^2R ligand environment, which is not consistent with any of the three possible isomers. No decoalescence of any of these resonances was observed between 298 and 220 K. Therefore, in order to elucidate the mode of ligand binding in **4**-**6**, a single crystal structure determination of one of these complexes was undertaken (see below).

Crystals of formula **5**·MeCN were grown from MeCN–Et_2O. The structure shows that the complex adopts a flattened tetrahedral geometry, with each ligand binding in a bidentate fashion through the pyridine N-donor and one imine group (Scheme 2, A; Fig. 4). While the two Cu–N bonds to one chelate ligand [Cu(1)–N(4) and Cu(1)–N(6)] are crystallographically identical (Table 4), the other ligand is bonded slightly asymmetrically, with Cu(1)–N(1) 2.0186(15) and Cu(1)–N(3) 2.0442(15) Å. The dihedral angle 'θ' between the planes of the two chelating ligands [Cu(1), N(1), N(3)] and [Cu(1), N(4), N(6)], which should be 90° for an 'ideal' tetrahedral geometry, is 71.2(2)°. This is within the range previously observed for other Cu^I/bis-diimine complexes, which often show distortions towards planarity with θ as low as 49°.[24] Although the pyridine ring and both imine groups of each ligand are essentially coplanar, the non-bonded imine groups of each ligand are rotated by *ca.* 180° about the C{*ipso*}–C{aldimine} single bond,

Table 4 Selected bond lengths (Å) and angles (°) for $[Cu(L^2Mes)_2]$-BF_4·MeCN **5**·MeCN

Cu(1)–N(1)	2.0186(15)	Cu(1)–N(4)	2.0292(15)
Cu(1)–N(3)	2.0442(15)	Cu(1)–N(6)	2.0344(15)
N(1)–Cu(1)–N(3)	81.85(6)	N(3)–Cu(1)–N(4)	128.45(6)
N(1)–Cu(1)–N(4)	123.13(6)	N(3)–Cu(1)–N(6)	106.98(6)
N(1)–Cu(1)–N(6)	139.88(6)	N(4)–Cu(1)–N(6)	82.52(6)

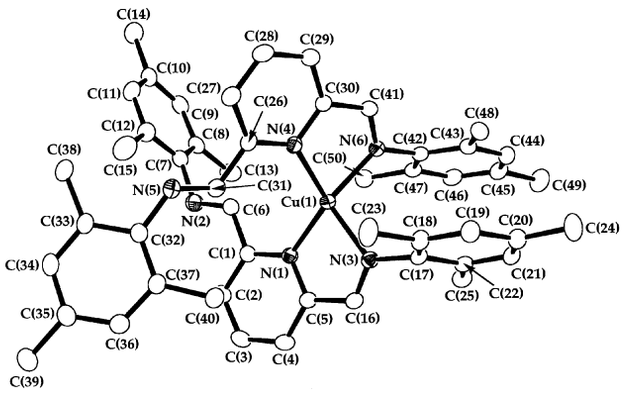

Fig. 4 View of the $[Cu(L^2Mes)_2]^+$ cation in the crystal of **5**·MeCN. Details as for Fig. 2.

so that the N atom lone pairs are oriented away from the copper ion. This ligand conformation enforces contacts between Cu(1) and the non-bonded aldimino C–H moieties of Cu(1)···H(6) 2.87 and Cu(1)···H(31) 2.90 Å.

There is an intramolecular stacking interaction between the two mesityl substituents C(17)–C(25) and C(42)–C(50) which are separated by 3.4 Å, the dihedral angle between the least squares planes of the two groups being 2.3(2)° and the centroids of the two phenyl rings being offset by 2.9 Å.[25] The relative orientations of the two groups places a methyl group above the centre of each phenyl ring, so that the distances between these C atoms C(25) and C(48) and the centroids of the neighbouring rings are 3.4–3.5 Å. This is suggestive of C-H-π interactions between these two groups, although confirmation of this by location of the methyl group H atoms in the difference map was not possible. There is an intermolecular π–π stacking interaction between the mesityl group C(32)–C(40) and C(32′)–C(40′) related by $1 - x$, $1 - y$, $1 - z$, which are strictly coplanar by symmetry, lie 3.4 Å apart and whose centroids are offset by 3.6 Å. The molecular structure of complex **5** is similar to that of $[Cu(L^2\{C_6H_4(OMe)\text{-}4\})_2]BF_4$, which was published during the course of this work.[13] This literature compound does not possess the intramolecular π–π interaction exhibited by **5** in the crystal, however, which leads it to adopt a more regular tetrahedral geometry with essentially perpendicular chelating ligands.

The deep colours of complexes **4**–**7** originate from one or two Cu→L^2R charge transfer absorptions.[23,26] For **4** this appears as a single peak $\lambda_{max} = 465$ nm ($\varepsilon_{max} = 2{,}200$ M^{-1} cm^{-1}), while for **6** and **7** it is split into two bands, at $\lambda_{max} = 455$ (sh) and 476 nm ($\varepsilon_{max} \approx 2{,}600$ M^{-1} cm^{-1} per L^2R ligand). For **5**, which bears aryl imine substituents, these peaks are weaker and at higher wavelengths, at $\lambda_{max} = 495$ ($\varepsilon_{max} = 881$) and 581 nm (367 M^{-1} cm^{-1}). The sensitivity of these MLCT absorptions to the identity of the L^2R substituent suggest that they represent transitions predominantly into the π* orbitals of the ligand aldimine moieties. The spectra of **4**–**7** also contain a second MLCT transition,[23] at $\lambda_{max} = 354$–369 nm ($\varepsilon_{max} = 1{,}600$–$10{,}500$ M^{-1} cm^{-1}), and lower wavelength π ⟶ π* transitions. The latter are substantially more complex than the π ⟶ π* region for **1**–**3**, consistent with the reduced symmetry of the asymmetrically co-ordinated L^2R ligands in **4**–**6**.

Cyclic voltammograms of complexes **4**–**7** were measured in MeCN–0.1 M $NBu^n_4BF_4$ at 298 K. All these compounds showed a chemically reversible Cu^{II}–Cu^{I} couple, at $E_{\frac{1}{2}} = -0.43$ (**4**), +0.19 (**5**), −0.31 (**6**) and −0.11 V (**7**) *vs.* ferrocene–ferrocenium. The potentials for **4**, **6** and **7** are broadly comparable to the reductions shown by related complexes such as $[Cu(L^1R)_2]^{2+}$ [*e.g.* $E_{pa}\{Cu^{II}$–$Cu^{I}\} = -0.06$ V for R = H and –0.45 V for R = Mes][27] or $[Cu(terpy)_2]^{2+}$ [21a,28] derivatives under similar conditions. However, the substantially more positive potential shown by **5** is consistent with the improved π-acceptor capability anticipated for L^2Mes compared to the alkyl-substituted L^2R ligands. Given the rather positive potential of the $[Cu(L^2Mes)_2]^{2+/+}$ couple, and since the brown colours obtained upon mixing copper(II) salts with L^2R (R = Ph or Mes) are visually identical to those of **4**–**7**, it is almost certain that our inability to prepare $[Cu(L^2R)_2]^{2+}$ with aryl 'R' groups reflects reduction of the copper(II) content of the reaction mixtures during complexation. In addition to the Cu^{II}–Cu^{I} couple, **4**–**7** also exhibit an irreversible Cu^{I}–Cu^{0} reduction at $E_{pc} = -1.79$ (**4**), −1.28 (**5**), −1.85 (**6**) and −1.90 V (**7**), with an associated oxidative desorption spike near –0.6 V reflecting deposition of copper metal at the electrode surface.

A copper(II) complex of L^3

We were keen to investigate whether a $\{d_{z^2}\}^1$ 6-co-ordinate copper(II) complex could be obtained without the use of bulky ligand substituents. We noted that the crystal structure of $[Fe(L^3)_2][PF_6]_2$ had been published previously, which showed that L^3 enforces extremely long Fe–N{pyridine} bonds in this complex.[29] This is a result of the inclusion of a 5-membered ring at the centre of the tridentate L^3 framework, rather than a 6-membered ring as in L^1R. We therefore suggested that conformational strain may induce correspondingly long Cu–N{pyridine bonds} in $[Cu(L^3)_2]^{2+}$, and that this would result in a $\{d_{z^2}\}^1$ ground state for this complex.

Complexation of $Cu(ClO_4)_2$·$6H_2O$ by 2 mol of L^3 in $MeNO_2$ yields a bright green solution, from which green microcrystals analysing as $[Cu(L^3)_2][ClO_4]_2$ **8** were obtained following concentration of the solution and addition of diethyl ether. Importantly, the IR spectrum of this compound was indistinguishable from those of its iron(II) and nickel(II) congeners,[29] which is consistent with the $[Cu(L^3)_2]^{2+}$ dication adopting a 6-co-ordinate structure in the solid, rather than an equally plausible 4-co-ordinate geometry with each ligand binding bidentately.[30] This proposal was confirmed by a crystal structure analysis.

Crystals of complex **8** give highly mosaic diffraction patterns, whose mosaicity increases upon cooling (see Experimental section). However, an analysis at room temperature was achieved of a poorly diffracting crystal of **8**, which is isomorphous with the high temperature form of $[Cu(L^1H)_2]$-$[BF_4]_2$.[5,7] Crystals of $[Cu(L^3)_2](BF_4)_2$ are also apparently isomorphous with these two salts but suffer from twinning, presenting an apparently tetragonal unit cell with $a = 8.7295(6)$ and $c = 37.461(2)$ Å at 150 K. The structure of **8** shows the complex to adopt the expected distorted octahedral stereochemistry, with two very short Cu–N{pyrazole} bonds of Cu(1)–N(2) 1.824(8) and Cu(1)–N(19) 1.838(9) Å (Fig. 5, Table 5). While the Cu(1)–N{pyridine} bonds to one L^3 ligand [N(2)–C(18)] are crystallographically indistinguishable (Table 5), the other ligand is bound rather asymmetrically with Cu(1)–N(25) 2.353(9) and Cu(1)–N(31) 2.233(9) Å. This asymmetric co-ordination is reflected in the chelate ring bite angles for this ligand, which are N(19)–Cu(1)–N(25) 69.8(3) and N(19)–Cu(1)–N(31) 76.5(3)°. All other metric parameters within the structure are unexceptional.

The powder EPR spectrum of complex **8** is very similar to that of **3**, with an almost axial $g_\perp > g_\parallel \approx g_e$ pattern whose parameters vary only slightly between 290 and 10 K (Table 1). As for **3**, this demonstrates that **8** has the desired $\{d_{z^2}\}^1$ ground

Table 5 Selected bond lengths (Å) and angles (°) for $[Cu(L^3)_2][ClO_4]_2$ **8**

Cu(1)–N(2)	1.824(8)	Cu(1)–N(19)	1.838(9)
Cu(1)–N(8)	2.297(8)	Cu(1)–N(25)	2.353(9)
Cu(1)–N(14)	2.326(8)	Cu(1)–N(31)	2.233(9)
N(2)–Cu(1)–N(8)	75.0(4)	N(8)–Cu(1)–N(31)	93.9(3)
N(2)–Cu(1)–N(14)	71.4(4)	N(14)–Cu(1)–N(19)	107.3(4)
N(2)–Cu(1)–N(19)	178.5(5)	N(14)–Cu(1)–N(25)	95.2(3)
N(2)–Cu(1)–N(25)	110.9(3)	N(14)–Cu(1)–N(31)	95.2(3)
N(2)–Cu(1)–N(31)	102.7(3)	N(19)–Cu(1)–N(25)	69.8(3)
N(8)–Cu(1)–N(14)	146.4(3)	N(19)–Cu(1)–N(31)	76.5(3)
N(8)–Cu(1)–N(19)	106.3(4)	N(25)–Cu(1)–N(31)	146.3(3)
N(8)–Cu(1)–N(25)	94.9(3)		

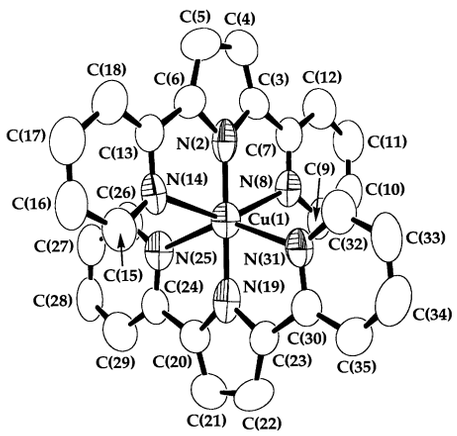

Fig. 5 View of the $[Cu(L^3)_2]^{2+}$ dication in the crystal of complex **8**. Details as for Fig. 2. The pyrrolic N atoms of the L^3 pyrazole rings are disordered over the C(3), C(6), C(20) and C(23) sites (see Experimental section).

state in the solid.[19] Interestingly, the parallel region of the spectrum becomes less well resolved as the temperature decreases, which is the opposite of the usual trend. The reason for this is uncertain, but may be related to the reduced crystallinity of **8** at lower temperatures (see above). In frozen MeCN or $MeNO_2$ solution, **8** affords a very different, poorly resolved EPR spectrum, which could not be simulated meaningfully but whose shape is suggestive of a tetragonal copper(II) species with $g_{\|} > g_{\perp} > g_e$.[19] Since **8** shows identical d–d maxima in MeCN and $MeNO_2$, the copper(II) ion does not undergo significant solvolysis in these solvents. Therefore, we tentatively propose that the solution EPR spectrum of **8** reflects partial isomerisation of the dissolved complex, to a [4 + 2] co-ordination geometry analogous to that shown by $[Cu(L^5)_2][BF_4]_2$ (L^5 = 3-{2,5-dimethoxyphenyl}-1-{pyridin-2-yl}pyrazole).[30] We note that the ^{1}H NMR spectrum of $[Ni(L^3)_2][BF_4]_2$[29] is much more complex than would be expected from its solid state structure, and demonstrates the presence of several paramagnetic species in solution.[27] It is likely that the solution structure of **8** is similarly complicated.

Concluding remarks

This study has established that our observation of sterically induced ground-state variability in $[Cu(L^1R)_2]^{2+}$ is not confined to this class of complexes, and appears to be general to other $[CuL_2]^{2+}$ systems where L is a meridional tris-imine ligand. This demonstrates an apparently general, but hitherto unreported, method by which the magnetic properties of a co-ordinated metal ion may be modulated by careful design of its steric environment. While there is little obvious applicability for these copper(II) systems, appropriate distal substitution of analogous $[FeL_2]^{2+}$ or $[CoL_2]^{2+}$ (L = meridional tris-imine ligand) may afford a new degree of control over the spin-crossover behaviour that is often exhibited by this class of compound. This would open new opportunities for the design of molecular magnetic switches or sensors. We are actively investigating these ideas.

Experimental

Unless stated otherwise, all manipulations were performed in air using commercial grade solvents. Pyridine-2,6-dicarbaldehyde,[31] L^2Ph,[16] L^2Bu′,[17] L^3[29] and $[Cu(NCMe)_4]BF_4$[32] were prepared by the literature procedures. $Cu(BF_4)_2{\cdot}6H_2O$ (Avocado), KH (Aldrich) and all solvents were used as supplied.

Syntheses

2,6-Bis(methyliminomethyl)pyridine (L^2Me). Pyridine-2,6-dicarbaldehyde (0.20 g, 1.5×10^{-3} mol) and methylamine (1.5 cm^3 of a 2 M solution in MeOH, 3.0×10^{-3} mol) were stirred in MeOH (25 cm^3) at room temperature for 1 h. The near-colourless solution was evaporated to dryness, leaving a yellow oil which formed a cream solid upon storage at −30 °C. Yield 0.21 g, 89% (Found: C, 66.9; H, 6.8; N, 26.3. Calc. for $C_9H_{11}N_3$: C, 67.1; H, 6.9; N, 26.1%). mp *ca.* 0 °C. EI mass spectrum: *m*/*z* 160, $[M - H]^+$; 146, $[M - CH_3]^+$; and 119, $[M - CHNCH_3]^+$. NMR spectra ($CDCl_3$, 293 K): ^{1}H; δ 8.37 (s, 2 H, HC=N), 7.91 (d, *J* 7.5, 2 H, Py H$^{3/5}$), 7.73 (t, *J* 7.5 Hz, 1H, Py H^4) and 3.53 (s, 6 H, CH_3); ^{13}C, δ 163.1 (HC=N), 154.3 (Py C$^{2/6}$), 137.1 (Py C^4), 122.1 (Py C$^{3/5}$) and 48.1 (CH_3).

2,6-Bis(2,4,6-trimethylphenyliminomethyl)pyridine (L^2Mes). Method as for L^2Me, using 2,4,6-trimethylphenylamine (0.40 g, 3.0×10^{-3} mol) but with a 1 h reflux. A yellow solid precipitated upon cooling the reaction mixture, which was filtered off, washed with MeOH and dried. Yield 0.48 g, 87% (Found: C, 81.0; H, 7.3; N, 11.5. Calc. for $C_{25}H_{27}N_3$: C, 81.3; H, 7.4; N, 11.4%). mp 156–158 °C. EI mass spectrum: *m*/*z* 369, $[M]^+$; 354, $[M - CH_3]^+$; 250, $[M - C_9H_{11}]^+$; and 236, $[M - NC_9H_{11}]^+$. NMR spectra ($CDCl_3$, 293 K): ^{1}H, δ 8.38 (s, 2 H, HC=N), 8.37 (d, *J* 7.5, 2 H, Py H$^{3/5}$), 7.94 (t, *J* 7.5 Hz, 1H, Py H^4), 6.89 (s, 4 H, Ph H$^{3/5}$), 2.28 (s, 6 H, 4-CH_3) and 2.14 (s, 12 H, 2,6-CH_3); ^{13}C, δ 163.1 (HC=N), 151.6 (Py C$^{2/6}$), 147.8 (Ph C^1), 137.7 (Py C^4), 133.5 (Ph C$^{2/6}$), 128.8 (Ph C$^{3/5}$), 126.8 (Ph C^4), 122.6 (Py C$^{3/5}$), 20.8 (4-CH_3) and 18.2 (2,6-CH_3).

2,6-Bis(cyclohexyliminomethyl)pyridine (L^2Cy). Method as for L^2Me, using cyclohexylamine (0.30 g, 3.0×10^{-3} mol). Following a 1 h reflux, the colourless solution was evaporated to dryness, leaving a tan oil which solidified upon standing at −30 °C. Yield 0.38 g, 87% (Found: C, 76.8; H, 9.4; N, 14.4. Calc. for $C_{19}H_{27}N_3$: C, 76.7; H, 9.2; N, 14.1%). mp *ca.* 25 °C. EI mass spectrum: *m*/*z* 297, $[M]^+$; and 214, $[M - C_6H_{11}]^+$. NMR spectra ($CDCl_3$, 293 K): ^{1}H; δ 8.46 (s, 2 H, HC=N), 8.05 (d, *J* 7.5, 2 H, Py H$^{3/5}$), 7.92 (t, 7.5 Hz, 1H, Py H^4), 3.35 (m, 2H, Cy CH) and 1.59 (m, 20H, Cy CH_2); ^{13}C, δ 159.4 (HC=N), 154.7 (Py C$^{2/6}$), 136.9 (Py C^4), 122.0 (Py C$^{3/5}$), 69.6 (Cy C^1), 34.2 (Cy C$^{2/6}$), 25.6 (Cy C$^{3/5}$) and 24.7 (Cy C^4).

Bis[2,6-bis(methyliminomethyl)pyridine]copper(II) bis(tetrafluoroborate) 1. A mixture of L^2Me (0.12 g, 7.70×10^{-4} mol) and $Cu(BF_4)_2{\cdot}6H_2O$ (0.13 g, 3.85×10^{-4} mol) was stirred in MeCN (20 cm^3) at room temperature for 30 min. The resultant dark brown-green solution was filtered and reduced to *ca.* 5 cm^3 volume. Vapour diffusion of Et_2O into this solution yielded oily green microcrystals. The supernatant was removed by decantation, and the solid washed twice with Et_2O and dried *in vacuo* to afford a green powder. Yield 0.090 g, 42% (Found: C, 38.5; H, 4.0; N, 14.9. Calc. for $C_{18}H_{22}B_2CuF_8N_6$: C, 38.6; H, 4.0; N, 15.0%). FAB mass spectrum: *m*/*z* 385, $[^{63}Cu(L^2Me)_2]^+$; and 224, $[^{63}Cu(L^2Me)]^+$. UV/vis spectrum: λ_{max}/nm (ε_{max}/M^{-1} cm^{-1})

(MeCN) 226 (33,700), 309 (8,100), 481 (sh) and 709 (48); ($MeNO_2$) 481 (sh) and 709 (50).

Bis[2,6-bis(cyclohexyliminomethyl)pyridine]copper(II) bis(tetrafluoroborate) 2. A solution of $Cu(BF_4)_2\cdot 6H_2O$ (0.13 g, 3.85×10^{-4} mol) and L^2Cy (0.23 g, 7.70×10^{-4} mol) in MeCN was stirred at room temperature for 30 min. The deep green solution was filtered and concentrated to *ca.* 5 cm^3 volume. Vapour diffusion of Et_2O into this solution formed green microcrystals, which were filtered off and dried. The product was recrystallised from $MeNO_2$–Et_2O. Yield 0.18 g, 55% (Found: C, 53.8; H, 6.8; N, 9.8. Calc. for $C_{38}H_{54}B_2CuF_8N_6\cdot H_2O$: C, 53.7; H, 6.6; N, 9.9%). FAB mass spectrum: *m/z* 657, $[^{63}Cu(L^2Cy)_2]^+$; 379, $[^{63}Cu(L^2Cy)F]^+$; and 360 $[^{63}Cu(L^2Cy)]^+$. UV/vis spectrum: λ_{max}/nm (ε_{max}/M^{-1} cm^{-1}) (MeCN) 226 (45,200), 308 (12,000), 478 (sh) and 709 (61); ($MeNO_2$): 478 (sh) and 706 (70).

Bis[2,6-bis(*tert*-butyliminomethyl)pyridine]copper(II) bis(tetrafluoroborate) 3. Method as for complex **2**, using L^2Bu^t (0.19 g, 7.70×10^{-4} mol). The product was recrystallised from $MeNO_2$–Et_2O. Yield 0.15 g, 52% (Found: C, 48.9; H, 6.4; N, 11.3. Calc. for $C_{30}H_{46}B_2CuF_8N_6$: C, 49.5; H, 6.4; N, 11.6%). FAB mass spectrum: *m/z* 553, $[^{63}Cu(L^2Bu^t)_2]^+$; and 308, $[^{63}Cu(L^2Bu^t)]^+$. UV/vis spectrum: λ_{max}/nm (ε_{max}/M^{-1} cm^{-1}) (MeCN) 243 (56,700), 274 (51,100) and 746 (63); ($MeNO_2$) 746 (62).

Bis[2,6-bis(methyliminomethyl)pyridine]copper(I) tetrafluoroborate 4. A solution of L^2Me (0.25 g, 1.55×10^{-3} mol) and $[Cu(NCMe)_4]BF_4$ (0.24 g, 7.75×10^{-4} mol) was stirred in MeCN (20 cm^3) at room temperature for 15 min. The dark brown solution was filtered and reduced to *ca.* 5 cm^3 volume. Vapour diffusion of Et_2O into this solution yielded dark brown microcrystals. Yield 0.26 g, 71% (Found: C, 45.1; H, 4.7; N, 17.2. Calc. for $C_{18}H_{22}BCuF_4N_6$: C, 45.7; H, 4.7; N, 17.8%). FAB mass spectrum: *m/z*, 385 $[^{63}Cu(L^2Me)_2]^+$; and 224, $[^{63}Cu(L^2Me)]^+$. UV/vis spectrum (MeCN): λ_{max}/nm (ε_{max}/M^{-1} cm^{-1}) 214 (47,100), 219 (41,600), 239 (13,700), 274 (sh), 285 (4,700) 294 (4,100), 362 (1,600) and 465 (2,200). ^1H NMR spectrum ($CDCl_3$, 293 K): δ 8.54 (s, 2 H, HC=N), 8.33 (t, *J* 6.6 Hz, 1 H, Py H^4), 8.21 (d, *J* 6.6 Hz, 2 H, Py $H^{3/5}$) and 3.43 (s, 6 H, CH_3).

Bis[2,6-bis(2,4,6-trimethylphenyliminomethyl)pyridine]copper(I) tetrafluoroborate 5. Method as for complex **4**, using L^2Mes (0.57 g, 1.55×10^{-3} mol). The product formed brown needles from MeCN–Et_2O. Yield 0.54 g, 78% (Found: C, 66.4; H, 6.2; N, 10.4. Calc. for $C_{50}H_{54}BCuF_4N_6\cdot CH_3CN$: C, 67.1; H, 6.2; N, 10.5%). FAB mass spectrum: *m/z* 801, $[^{63}Cu(L^2Mes)_2]^+$; and 432, $[^{63}Cu(L^2Mes)]^+$. UV/vis spectrum (MeCN): λ_{max}/nm (ε_{max}/M^{-1} cm^{-1}) 225 (65,400), 234 (68,100), 283 (24,900), 354 (10,500), 495 (881) and 581 (367). ^1H NMR spectrum ($CDCl_3$, 293 K): δ 8.53 (s, 2 H, HC=N), 8.48 (d, *J* 6.4, 2 H, Py $H^{3/5}$), 8.42 (t, *J* 6.4 Hz, 1 H, Py H^4), 6.79 (s, 4 H, Ph $H^{3/5}$), 2.21 (s, 6 H, 4-CH_3) and 1.74 (s, 12 H, 2,6-CH_3).

Bis[2,6-bis(cyclohexyliminomethyl)pyridine]copper(I) tetrafluoroborate 6. Method as for complex **4**, using L^2Cy (0.46 g, 1.55×10^{-3} mol). The product formed a dark brown solid from MeCN–EtO_2. Yield 0.45 g, 78% (Found: C, 61.0; H, 7.0; N, 11.2. Calc. for $C_{38}H_{54}BCuF_4N_6$: C, 61.2; H, 6.8; N, 11.3%). FAB mass spectrum: *m/z* 657, $[^{63}Cu(L^2Cy)_2]^+$; and 360, $[^{63}Cu(L^2Cy)]^+$. UV/vis spectrum (MeCN): λ_{max}/nm (ε_{max}/M^{-1} cm^{-1}) 220 (43,200), 246 (20,800), 279 (sh), 285 (17,900), 368 (1,900), 455 (sh) and 476 (4,600). ^1H NMR spectrum ($CDCl_3$, 293 K): δ 8.39 (s, 2 H, HC=N), 8.14 (m, 3 H, Py $H^{3/4/5}$), 3.27 (m, 2 H, Cy CH), 1.56 (m, 10 H, Cy CH_2) and 1.13 (m, 10 H, Cy CH_2).

Bis[2,6-bis(*tert*-butyliminomethyl)pyridine]dicopper(I) bis(tetrafluoroborate) 7. Method as for complex **4**, using L^2Bu^t (0.19 g, 7.75×10^{-4} mol). The product formed deep red needles from $MeNO_2$–Et_2O. Yield 0.19 g, 63% (Found: C, 43.5; H, 5.7; N, 10.2. Calc. for $C_{15}H_{23}BCuF_4N_3\cdot H_2O$: C, 43.7; H, 5.9; N, 10.2%). FAB mass spectrum: *m/z* 616, $[^{63}Cu_2(L^2Bu^t)_2]^+$; 395, $[^{63}Cu(L^2Bu^t)^{11}BF_4]^+$; and 308, $[^{63}Cu(L^2Bu^t)]^+$. UV/vis spectrum (MeCN): λ_{max}/nm (ε_{max}/M^{-1} cm^{-1}) 217 (41,000), 240 (24,700), 273 (sh), 283 (15,443), 369 (2,400), 455 (sh) and 476 (2,700). ^1H NMR spectrum ($CDCl_3$, 293 K): δ 8.71 (s, 2H, HC=N), 8.37 (m, 3H, Py $H^{3/4/5}$) and 1.21 (s, 18H, CH_3).

Bis(1,3-bis{pyridin-2-yl}pyrazole)copper(II) diperchlorate 8. A solution of L^3 (0.50 g, 2.25×10^{-3} mol) and $Cu(ClO_4)_2\cdot 6H_2O$ (0.42 g, 1.13×10^{-3} mol) in $MeNO_2$ (20 cm^3) was stirred at room temperature for 30 min. The intensely green solution was filtered and reduced to *ca.* 5 cm^3 volume. Vapour diffusion of Et_2O into this solution yielded deep green microcrystals. Yield 0.54 g, 68% (Found: C, 44.1; H, 2.9; N, 16.2. Calc. for $C_{26}H_{20}Cl_2CuN_8O_8$: C, 44.2; H, 2.9; N, 15.9%). FAB mass spectrum: *m/z* 507, $[^{63}Cu(L^3)_2]^+$; 285, $[^{63}Cu(L^3)]^+$; and 223, $[L^3H]^+$. UV/vis spectrum: λ_{max}/nm (ε_{max}/M^{-1} cm^{-1}) (MeCN) 220 (sh), 227 (sh), 249 (23,000), 255 (sh), 270 (20,700), 277 (20,000), 307 (35,700), 320 (sh), 368 (sh), 415 (sh) and 761 (119); ($MeNO_2$): 415 (sh) and 761 (129). **CAUTION**: although we have experienced no difficulties in handling complex **8**, metal–organic perchlorates are potentially explosive and should be treated with due care.

Bis(1,3-bis{pyridin-2-yl}pyrazole)copper(II) bis(tetrafluoroborate). Method as for complex **8**, using $Cu(BF_4)_2\cdot 6H_2O$ (0.39 g, 1.13×10^{-3} mol). Yield 0.55 g, 71% (Found: C, 46.0; H, 3.0; N, 16.4. Calc. for $C_{26}H_{20}B_2CuF_8N_8$: C, 45.8; H, 3.0; N, 16.4%).

Single crystal structure determinations

Single crystals of X-ray quality of $[Cu(L^2Cy)_2][BF_4]_2\cdot MeNO_2$ **2**·$MeNO_2$, $[Cu(L^2Bu^t)_2][BF_4]_2\cdot\frac{1}{2}Me_2CO$ **3**·$\frac{1}{2}Me_2CO$ and $[Cu(L^2Mes)_2]BF_4\cdot MeCN$ **5**·MeCN were grown by diffusion of ether vapour into solutions of the complexes in the appropriate solvents. Crystals of $[Cu(L^3)_2][ClO_4]_2$ **8** were similarly grown from $MeNO_2$–Et_2O. Experimental details from the structure determinations are given in Table 6. All structures were solved by direct methods (SHELXS 86[33]) and refined by full matrix least squares on F^2 (SHELXL 97[34]), with H atoms placed in calculated positions.

$[Cu(L^2Cy)_2][BF_4]_2\cdot MeNO_2$ 2·$MeNO_2$. The F atoms of one BF_4^- anion were disordered, and were modelled using two orientations in a 60:40 occupancy ratio with the B–F distances restrained to 1.36(2) Å. A badly disordered region of solvent lying across a crystallographic 2-fold axis, which could not be identified unambiguously, was modelled using 4 half-occupied carbon environments. All non-H atoms with occupancy >0.5 were refined anisotropically.

$[Cu(L^2Bu^t)_2][BF_4]_2\cdot\frac{1}{2}Me_2CO$ 3·$\frac{1}{2}Me_2CO$. The asymmetric unit contains 2 complex cations, 4 BF_4^- anions and one molecule of acetone. All non-H atoms were refined anisotropically, and no disorder was detected.

$[Cu(L^2Mes)_2]BF_4\cdot MeCN$ 5·MeCN. During refinement, the BF_4^- anion was found to be disordered over three sites, which were modelled with a 50:30:20 occupancy ratio with all B–F distances restrained to 1.38(2) Å, and F···F distances to 2.25(2) Å. All non-H atoms with occupancy ≥0.5 were refined anisotropically.

$[Cu(L^3)_2][ClO_4]_2$ 8. All crystals of this compound that were examined had a high mosaicity, which increased upon cooling. The crystal used for data collection had a mosaicity of 0.914(3) at 293 K, compared to a more typical value of 0.4–0.5. Both perchlorate anions were disordered over two distinct orienta-

Table 6 Experimental details for the single crystal structure determinations

	$[Cu(L^2Cy)_2][BF_4]_2\cdot MeNO_2$ **2**·$MeNO_2$	$[Cu(L^2Bu^t)_2][BF_4]_2\cdot\frac{1}{2}Me_2CO$ **3**·$\frac{1}{2}Me_2CO$	$[Cu(L^2Mes)_2]BF_4\cdot MeCN$ **5**·MeCN	$[Cu(L^3)_2][ClO_4]_2$ **8**
Formula	$C_{39}H_{57}B_2CuF_8N_7O_2$	$C_{31.5}H_{49}B_2CuF_8N_6O_{0.5}$	$C_{52}H_{57}BCuF_4N_7$	$C_{26}H_{20}Cl_2CuN_8O_8$
M_r	917.10	756.93	930.40	706.94
Crystal class	Monoclinic	Triclinic	Monoclinic	Monoclinic
Space group	$P2_1/c$	$P\bar{1}$	$P2_1/c$	$P2_1$
a/Å	13.6323(1)	11.1235(1)	11.6577(2)	8.753(2)
b/Å	17.8182(1)	17.0639(2)	26.3758(4)	8.789(2)
c/Å	19.2083(1)	19.9979(3)	16.2105(2)	19.381(5)
α/°	—	81.6900(8)	—	—
β/°	104.5180(6)	75.7200(8)	105.1990(10)	92.334(14)
γ/°	—	89.0990(8)	—	—
U/Å^3	4516.77(5)	3639.12(8)	4809.96(13)	1489.7(6)
Z	4	4	4	2
μ(Mo-Kα)/mm^{-1}	0.559	0.674	0.513	0.975
T/K	150(2)	150(2)	150(2)	293(2)
Measured reflections	70847	114065	114573	7778
Independent reflections	8844	16691	10969	4711
R_{int}	0.050	0.064	0.098	0.061
$R(F)$	0.056	0.043	0.042	0.089
$wR(F^2)$	0.159	0.127	0.111	0.260
S	1.043	1.027	1.024	1.066
Flack parameter	—	—	—	0.04(4)

tions, which were modelled with occupancy ratios of 60:40 (anion 1) and 80:20 (anion 2). All Cl–O distances were restrained to 1.39(2) Å and non-bonded O···O distances to 2.27(2) Å, while individual U_{ij} parameters for each O atom were restrained to be the same with an esd of 0.04 Å^2; rigid bond restraints were also applied to these thermal parameters. The resolution of the structure was too low to distinguish between the pyrazole N1 and C3 sites on the L^3 ligands, which could in any case be disordered.[29] Hence these sites in the structure, namely C(3), C(6), C(20) and C(23), were all refined as C atoms. All non-H atoms except the minor disorder orientation of anion 2 were refined anisotropically.

CCDC reference number 186/2129.

See http://www.rsc.org/suppdata/dt/b0/b005105p/ for crystallographic files in .cif format.

Other measurements

Infrared spectra were obtained as Nujol mulls pressed between KBr windows between 400 and 4000 cm^{-1} using a Nicolet Avatar 360 spectrophotometer, UV/visible spectra with a Perkin-Elmer Lambda 900 spectrophotometer in 1 cm quartz cells, NMR spectra on a Bruker ARX250 spectrometer operating at 250.1 (^{1}H) and 62.9 MHz (^{13}C), electron impact and positive ion fast atom bombardment mass spectra on a VG AutoSpec spectrometer, the FAB spectra employing a 3-nitrobenzyl alcohol matrix. CHN microanalyses were performed by the University of Leeds School of Chemistry microanalytical service. Melting points are uncorrected. EPR spectra were obtained using a Bruker ESP300E spectrometer, fitted with an ER5106QT Q-band resonator and an ER4118VT cryostat. Spectral simulations were performed using in-house software which has been described elsewhere.[35]

All electrochemical measurements were carried out using an Autolab PGSTAT30 voltammetric analyser, in MeCN containing 0.1 M $NBu^n_4BF_4$ (prepared from NBu^n_4OH and HBF_4) as supporting electrolyte. Cyclic voltammetric experiments involved the use of platinum working and counter electrodes and an Ag–AgCl reference electrode; all potentials quoted are referenced to an internal ferrocene–ferrocenium standard and were obtained at a scan rate of 100 mV s^{-1}.

Acknowledgements

The authors thank Dr Michael Hitchman (University of Tasmania) for useful discussions. Financial support is acknowledged from the Royal Society (research fellowship to MAH), the EPSRC and the University of Leeds.

References

1 L. R. Falvello, *J. Chem. Soc.*, *Dalton Trans.*, 1997, 4463.
2 J.-V. Folgado, W. Henke, R. Allmann, H. Stratemeier, D. Beltrán-Porter, T. Rojo and D. Reinen, *Inorg. Chem.*, 1990, **29**, 2035.
3 M. Duggan, B. J. Hathaway and J. Mullane, *J. Chem. Soc.*, *Dalton Trans.*, 1980, 690.
4 J. H. Ammeter, H. B. Bürgi, E. Gamp, V. Meyer-Sandrin and W. P. Jensen, *Inorg. Chem.*, 1979, **18**, 733.
5 N. K. Solanki, E. J. L. McInnes, F. E. Mabbs, S. Radojevic, M. McPartlin, N. Feeder, J. E. Davies and M. A. Halcrow, *Angew. Chem.*, *Int. Ed.*, 1998, **37**, 2221.
6 M. A. Leech, N. K. Solanki, M. A. Halcrow, J. A. K. Howard and S. Dahaoui, *Chem. Commun.*, 1999, 2245.
7 A. J. Bridgeman, M. A. Halcrow, M. Jones, E. Krausz and N. K. Solanki, *Chem. Phys. Lett.*, 1999, **314**, 176.
8 C. J. Simmons, *New J. Chem.*, 1993, **17**, 77.
9 G. Wingefeld and R. Hoppe, *Z. Anorg. Allg. Chem.*, 1984, **516**, 223; K. Finnie, L. Dubicki, E. R. Krausz and M. J. Riley, *Inorg. Chem.*, 1990, **29**, 3908; M. Atanasov, M. A. Hitchman, R. Hoppe, K. S. Murray, B. Moubaraki, D. Reinen and H. Stratemeier, *Inorg. Chem.*, 1993, **32**, 3397; V. M. Masters, M. J. Riley and M. A. Hitchman, *J. Synchrotron Rad.*, 1999, **6**, 242.
10 F. Lions and K. V. Martin, *J. Am. Chem. Soc.*, 1957, **79**, 2733.
11 G. J. P. Britovsek, V. C. Gibson, B. S. Kimberley, P. J. Maddox, S. J. McTavish, G. A. Solan, A. J. P. White and D. J. Williams, *Chem. Commun.*, 1998, 849.
12 A. L. Vance, N. W. Alcock, J. A. Heppert and D. H. Busch, *Inorg. Chem.*, 1998, **37**, 6912.
13 L. Douce, A. El-ghayoury, A. Skoulios and R. Zeissel, *Chem. Commun.*, 1999, 2033.
14 P. H. Merrell, E. C. Alyea and L. Ecott, *Inorg. Chim. Acta*, 1982, **59**, 25; M. S. Nelson, A. J. Lavery and M. G. B. Drew, *J. Chem. Soc.*, *Dalton Trans.*, 1986, 911.
15 A. J. Blake, A. J. Lavery, T. I. Hyde and M. Schröder, *J. Chem. Soc.*, *Dalton Trans.*, 1989, 965.
16 T. W. Bell, F. Guzzo and M. G. B. Drew, *J. Am. Chem. Soc.*, 1991, **113**, 3115.
17 J. Mlochowski, E. Kubicz, K. Kloc, M. Mordarski, W. Peczynska and L. Syper, *Liebigs Ann. Chem.*, 1988, 455.
18 A. B. P. Lever, *Inorganic Electronic Spectroscopy*, 2nd edn., Elsevier, Amsterdam, 1984, pp. 554–572.
19 B. A. Goodman and J. B. Raynor, *Adv. Inorg. Chem.*, 1970, **13**, 135.
20 N. K. Solanki, A. E. H. Wheatley, S. Radojevic, M. McPartlin and M. A. Halcrow, *J. Chem. Soc.*, *Dalton Trans.*, 1999, 521.
21 (*a*) K. T. Potts, M. Kesharvaz-K, F. S. Tham, H. D. Abruña and C. Arana, *Inorg. Chem.*, 1993, **32**, 4450; (*b*) E. C. Constable, A. J. Edwards, M. J. Hannon and P. R. Raithby, *J. Chem. Soc.*, *Chem. Commun.*, 1994, 1991; (*c*) E. C. Constable, T. Kulke, M. Neuberger and M. Zehnder, *Chem. Commun.*, 1997, 489.

22 C. Piguet, G. Bernardinelli and A. F. Williams, *Inorg. Chem.*, 1989, **28**, 2920; S. Rüttiman, C. Piguet, G. Bernardinelli, B. Bocquet and A. F. Williams, *J. Am. Chem. Soc.*, 1992, **114**, 4230; R. F. Carina, G. Bernardinelli and A. F. Williams, *Angew. Chem., Int. Ed. Engl.*, 1993, **32**, 1463; R. E. Carina, A. F. Williams and C. Piguet, *Helv. Chim. Acta*, 1998, **81**, 548.
23 M. G. B. Drew, A. Lavery, V. McKee and S. M. Nelson, *J. Chem. Soc., Dalton Trans.*, 1985, 1771.
24 For recent examples see *e.g.* S. M. Scott, K. C. Gordon and A. K. Burrell, *Inorg. Chem.* 1996, **35**, 2452; M. K. Eggleston, P. E. Fanwick, A. J. Pallenberg and D. R. McMillin, *Inorg. Chem.*, 1997, **36**, 4007; M. A. Halcrow, N. L. Cromhout and P. R. Raithby, *Polyhedron*, 1997, **16**, 4257; M. T. Miller, P. K. Gantzel and T. B. Karpishin, *Inorg. Chem.*, 1998, **37**, 2285; M. T. Miller, P. K. Gantzel and T. B. Karpishin, *Inorg. Chem.*, 1999, **38**, 3414; C. L. Foster, C. A. Kilner, M. Thornton-Pett and M. A. Halcrow, *Acta Crystallogr., Sect. C*, 2000, **56**, 319.
25 C. A. Hunter and J. K. M. Sanders, *J. Am. Chem. Soc.*, 1990, **112**, 5525.
26 K. T. Potts, M. Kesharvaz-K, F. S. Tham, H. D. Abruña and C. R. Arana, *Inorg. Chem.*, 1993, **32**, 4422; K. T. Potts, M. Kesharvaz-K, F. S. Tham, H. D. Abruña and C. R. Arana, *Inorg. Chem.*, 1993, **32**, 4436.
27 N. K. Solanki and M. A. Halcrow, unpublished data.
28 G. D. Storrier, S. B. Colbran and D. C. Craig, *J. Chem. Soc., Dalton Trans.*, 1998, 1351; M. A. Halcrow, E. K. Brechin, E. J. L. McInnes, F. E. Mabbs and J. E. Davies, *J. Chem. Soc., Dalton Trans.*, 1998, 2477.
29 A. T. Baker, D. C. Craig, G. Dong and A. D. Rae, *Aust. J. Chem.*, 1995, **48**, 1071.
30 M. A. Halcrow, E. J. L. McInnes, F. E. Mabbs, I. J. Scowen, M. McPartlin, H. R. Powell and J. E. Davies, *J. Chem. Soc., Dalton Trans.*, 1997, 4025.
31 N. W. Alcock, R. G. Kingston, P. Moore and C. Pierpoint, *J. Chem. Soc., Dalton Trans.*, 1984, 1937.
32 G. J. Kubas, *Inorg. Synth.*, 1990, **28**, 68.
33 G. M. Sheldrick, *Acta Crystallogr., Sect. A*, 1990, **46**, 467.
34 G. M. Sheldrick, SHELXL 97, Program for the refinement of crystal structures, University of Göttingen, 1997.
35 F. E. Mabbs and D. Collison, *Electron Paramagnetic Resonance of d Transition Metal Compounds*, Elsevier, Amsterdam, 1992, ch. 7.